ORNL/TM-2023/3214

SCALE Demonstration for Sodium-Cooled Fast Reactor Fuel Cycle Analysis

Donny Hartanto
Georgeta Radulescu
Friederike Bostelmann
Rabab Elzohery
William Wieselquist

Approved for public release.
Distribution is unlimited.

April 2024

OAK RIDGE National Laboratory

ORNL IS MANAGED BY UT–BATTELLE, LLC, FOR THE U.S. DEPARTMENT OF ENERGY

DOCUMENT AVAILABILITY

Reports produced after January 1, 1996, are generally available free via US Department of Energy (DOE) SciTech Connect.

Website osti.gov

Reports produced before January 1, 1996, may be purchased by members of the public from the following source:

National Technical Information Service
5285 Port Royal Road
Springfield, VA 22161
Telephone 703-605-6000 (1-800-553-6847)
TDD 703-487-4639
Fax 703-605-6900
E-mail info@ntis.gov
Website classic.ntis.gov

Reports are available to DOE employees, DOE contractors, Energy Technology Data Exchange representatives, and International Nuclear Information System representatives from the following source:

Office of Scientific and Technical Information
PO Box 62
Oak Ridge, TN 37831
Telephone 865-576-8401
Fax 865-576-5728
E-mail reports@osti.gov
Website osti.gov

This report was prepared as an account of work sponsored by an agency of the United States Government. Neither the United States Government nor any agency thereof, nor any of their employees, makes any warranty, express or implied, or assumes any legal liability or responsibility for the accuracy, completeness, or usefulness of any information, apparatus, product, or process disclosed, or represents that its use would not infringe privately owned rights. Reference herein to any specific commercial product, process, or service by trade name, trademark, manufacturer, or otherwise, does not necessarily constitute or imply its endorsement, recommendation, or favoring by the United States Government or any agency thereof. The views and opinions of authors expressed herein do not necessarily state or reflect those of the United States Government or any agency thereof.

ORNL/TM-2023/3214

Nuclear Energy and Fuel Cycle Division

SCALE DEMONSTRATION FOR SODIUM-COOLED FAST REACTOR FUEL CYCLE ANALYSIS

Donny Hartanto
Georgeta Radulescu
Friederike Bostelmann
Rabab Elzohery
William Wieselquist

April 2024

Prepared by
OAK RIDGE NATIONAL LABORATORY
Oak Ridge, TN 37831-6283
managed by
UT-Battelle, LLC
for the
US DEPARTMENT OF ENERGY
under contract DE-AC05-00OR22725

CONTENTS

LIST OF FIGURES

LIST OF TABLES

ABBREVIATIONS

ABTR	Advanced Burner Test Reactor
ANL	Argonne National Laboratory
CB	containment building
EBR-II	Experimental Breeder Reactor II
ER	electrorefiner
FP	fission product
HALEU	high-assay low-enriched U
non-LWR	non-light-water reactor
NRC	Nuclear Regulatory Commission
ORNL	Oak Ridge National Laboratory
PWR	pressurized water reactor
SFR	sodium-cooled fast reactor
SS	stainless steel
TRU	transuranic
U/TRU	U/transuranic

ACKNOWLEDGMENTS

Support for this work was provided by the US Nuclear Regulatory Commission under Contract IAA 31310022S0011. The authors thank Cihangir Celik for the technical review of the report.

ABSTRACT

In support of the US Nuclear Regulatory Commission non-light-water reactor fuel cycle demonstration project, SCALE 6.3.1 capabilities for radionuclide characterization, criticality, and shielding were demonstrated for scenarios in the sodium-cooled fast reactor (SFR) nuclear fuel cycle. Three postulated accident scenarios were selected for analysis in this work. As a basis for all scenarios, irradiated fuel inventories were generated using SCALE/ORIGAMI. To cover multiple SFR design choices, two different types of SFR fuel, uranium/transuranic-loaded and U-based fuels, were considered. For the first scenario, SCALE/MAVRIC was used to calculate the radiation shielding and dose rates inside and outside of the containment building due to a drop of a spent fuel assembly from the fuel-handling system during unloading inside the containment building. For the second scenario, potential critical configurations in an electrofiner were investigated through criticality calculations with SCALE/CSAS. For the third scenario, the activity of the waste salt from an electrorefiner was evaluated using SCALE/ORIGEN. The dose rate produced by the analyzed SFR assemblies is similar to that produced by a typical pressurized water reactor (PWR) fuel assembly with a discharge burnup of 50 GWd/MTU, with the same cooling time of 10 days. The criticality analyses suggested that the different electrorefiner configurations have a large margin to criticality. The activity analysis of the electrofiner waste revealed that shielding and cooling may be required for the waste salt that contains transuranics and fission products produced by the electrorefiner because of the high activity of the waste salt. In general, the application of various capabilities in the SCALE code system for SFR fuel inventory generation, criticality, and shielding was successfully demonstrated for the selected scenarios in the SFR nuclear fuel cycle. Additional analyses can be performed to provide more accurate results when more details of the SFR nuclear fuel cycles are available, for example, the dimension of the electrorefiner and the salt compositions during reprocessing,

1. INTRODUCTION

The US Nuclear Regulatory Commission (NRC) has been supporting the evaluation of computer code capabilities for modeling accident-progression, source-term, and consequence analysis in non-light-water reactor (non-LWR) systems (US NRC 2020a). With the goal of helping meet the licensing needs in the near future, the computer codes SCALE (Wieselquist and Lefebvre 2023) and MELCOR (Humphries et al. 2021) were evaluated for relevant non-LWR applications. The SCALE code system, developed at Oak Ridge National Laboratory (ORNL), is used for radionuclide characterization, criticality analyses, and shielding analyses, whereas the MELCOR code, developed by Sandia National Laboratories, performs severe accident-progression and source-term analyses for accident scenarios using the nuclide inventories and decay heat generated by SCALE. The modeling and simulation capabilities of these codes for non-LWRs have been demonstrated, including for heat pipe reactors (Walker et al. 2021; Wagner, Faucett, et al. 2022), high-temperature pebble-bed gas-cooled reactors (Wagner, Beeny, and Luxat 2022; Skutnik and Wieselquist 2021), fluoride-salt-cooled high-temperature reactors (Bostelmann et al. 2022; Wagner, Haskin, et al. 2022), molten-salt-fueled reactors (Lo et al. 2022; Wagner et al. 2023), and sodium-cooled fast reactors (SFRs) (Shaw et al. 2023; Wagner, Beeny, and Luxat 2023).

Following these initial efforts, a new NRC project supports the demonstration of computer code capabilities for radionuclide inventory characterization, criticality analyses, and shielding analyses in all fuel cycle stages of non-LWRs (US NRC 2021). The first task for this project was to develop representative nuclear fuel cycles for five non-LWR designs and to identify potential hazards and accident scenarios in the individual fuel cycle stages summarized by Bostelmann et al. (2023). Individual accident scenarios from this work were selected for the demonstration of capabilities for SCALE and MELCOR. The accident scenarios were thereby selected based on their suitability to be used for code demonstration but independently of their probability to occur. The first demonstration was carried out for the safety of a high-temperature pebble-bed gas-cooled reactor fuel cycle using SCALE and MELCOR (US NRC, ORNL, SNL 2023). The present report documents the second demonstration for an SFR. The 250 MWth Advanced Burner Test Reactor (ABTR) was selected as the reference design to leverage the previous modeling efforts (Shaw et al. 2023).

The ABTR is a conceptual pool-type SFR design using U/transuranic (U/TRU) metallic fuel, developed by Argonne National Laboratory (ANL) (Chang, Finck, and Grandy 2006; Kim 2020). It is intended to demonstrate the safety of SFRs, demonstrate the transmutation of transuranics (TRUs), and qualify the TRU-containing fuel in an SFR. As illustrated in Figure 1, the reactor core comprises 54 fuel assemblies, 78 reflector assemblies, 48 shield assemblies, 10 control rod assemblies, and 9 test assemblies. The fuel assemblies are divided into inner and outer regions with different TRU enrichments to flatten the radial power distributions. The U/TRU isotopic composition of the driver fuel assembly is obtained from weapons-grade Pu, and the test fuel assembly uses U/TRUs from 10-year cooled light-water reactor spent fuel with burnup of 33 GWd/tHM. The reactor core operates following multibatch refueling with a cycle length of 4 months.

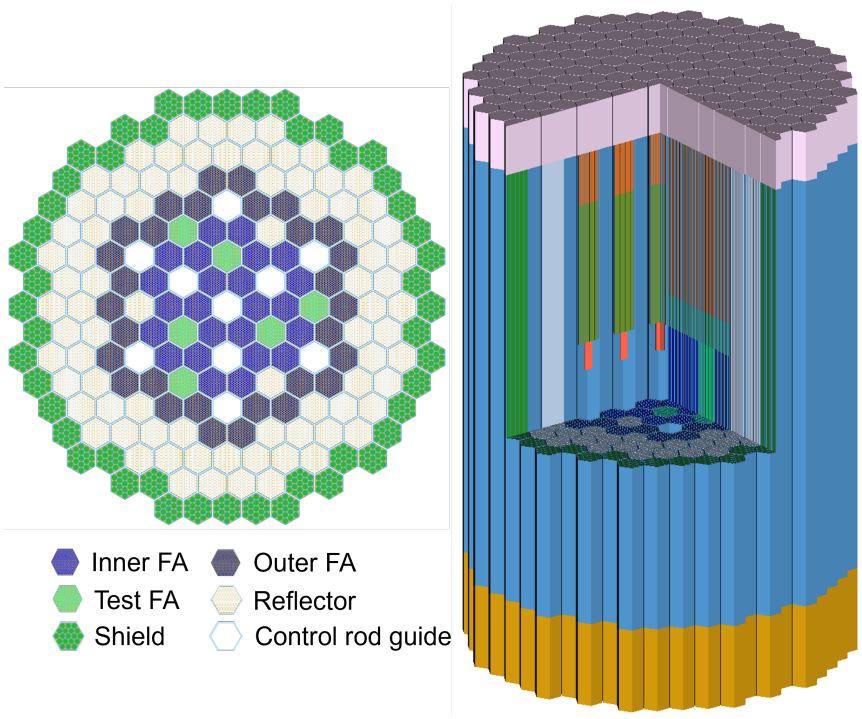

Figure 1. SCALE ABTR-250 model.

The demonstration of the SCALE code to analyze the safety of SFR nuclear fuel cycles was performed in three accident scenarios, which included:

- Release of fission products during operation/refueling. A seismic event or earthquake was assumed, causing the refueling machine to fall and release the fuel assembly. The radiation doses inside and outside reactor containment due to the unshielded fuel assembly were calculated.
- Fissile material buildup during reprocessing. The misfeed of material into the electro-processing batch was assumed, leading to fissile material buildup on the cathode. The criticality calculations of an electrorefiner due to the fissile misfeed were calculated.
- Release of fission products during reprocessing. A leak in the waste stream storage tank was assumed and allowed the release of fission products during reprocessing. The activity of the waste stream was evaluated.

While nuclear fuel reprocessing is presently not implemented in the United States, it is covered in this study. Its crucial role in the closed fuel cycles, as exemplified in the historical operation of the Experimental Breeder Reactor II, highlights its importance.

2. SCALE CODE APPLICATIONS

The SCALE code system includes analysis sequences for reactor physics, depletion, criticality, shielding, and cross section sensitivity/uncertainty calculations. The work described in this report was accomplished mainly using four sequences of SCALE 6.3.1.

- SCALE/TRITON was used to generate the ORIGEN reactor libraries. ORIGEN reactor libraries are sets of ORIGEN one-group cross section libraries for specific reactor types and fuel assembly configurations, parameterized to relevant conditions such as fuel enrichment and burnup histories.
- SCALE/ORIGAMI was used to obtain the spent fuel inventories in each accident scenario. This sequence rapidly computes detailed irradiated and decayed isotopic compositions using the ORIGEN transmutation solver based on pregenerated ORIGEN reactor libraries. It also provides the decay heat, activity, and radiation source terms of the spent fuel. Additionally, it can be used to consider the activation of the irradiated nonfuel materials, such as the cladding and structural materials. SCALE/ORIGEN can be used as a stand-alone code or within other modules to perform depletion and decay calculations.
- SCALE/MAVRIC was used to perform the shielding and radiation dose calculations (Peplow 2011). The shielding analysis sequence uses the MONACO module for Monte Carlo photon and neutron transport calculations. It can automatically generate variance reduction parameters based on input specifications for shielding analyses. The variance reduction methods implemented in MAVRIC significantly increase the figure of merit of Monte Carlo transport calculations by systematically reducing statistical uncertainties and computational time (Peplow 2011; Wagner, Peplow, and Mosher 2014; Evans et al. 2010). Radiation source terms determined with depletion and decay modules in SCALE can be directly accessed by MAVRIC, which reduces the complexity of input specifications.
- SCALE/CSAS was used to conduct the criticality calculations. This sequence uses the Monte Carlo neutron code KENO or Shift to evaluate the multiplication factor of a system.

3. SPENT FUEL INVENTORY GENERATION

The inventory of spent nuclear fuel is essential for evaluating radiation source terms in modeled accident scenarios. The present study generated spent fuel inventories for radiation source terms from the ABTR and a typical pressurized water reactor (PWR). The spent fuels encompassed four types, as summarized in Table 1. The ABTR U/TRU metallic fuel contained weapons-grade plutonium (Chang, Finck, and Grandy 2006), with differing TRU contents for the inner and outer fuel assemblies. Specifically, the inner fuel assembly contained a lower TRU content of 16.5 wt %, whereas the outer fuel assembly used a slightly higher TRU content of 20.7 wt %. Furthermore, the inner fuel assembly was irradiated with comparatively high specific power and achieved slightly higher discharged burnup than the outer fuel assembly. However, subsequent analysis revealed that the ABTR inner and outer fuels exhibited similar decay heat and activity characteristics. Therefore, only the ABTR inner fuel assembly was adopted as the radiation source terms in the modeled accident scenarios.

Table 1. Initial fuel compositions and irradiation histories of spent nuclear fuels

Parameter	ABTR U/TRU Inner	ABTR U/TRU Outer	ABTR HALEU	PWR
Fuel	U/TRU-10Zr	U/TRU-10Zr	U-10Zr	UO_2
Fuel density (g/cm^3)	11.37	11.37	11.37	10.40
Fuel enrichment (wt %)	16.5% TRU	20.7% TRU	16.5% ^{235}U	4.20% ^{235}U
Heavy metal per assembly (kg)	72.193	72.193	72.193	459.52
Specific power (GW/tHM)	65.62	51.46	46.22	33.70
Irradiation length (cycles)	12	15	6	3
Cycle length (days)	120	120	540	494.56
Cooling between cycle (days)	10	10	10	24.73
Discharged burnup (GWd/tHM)	94.50	92.60	149.74	50.00
Applied scenarios	All	—	All	2 and 3

In addition to using U/TRU metallic fuel, this study considered the operation of ABTR with fresh U-10Zr metallic fuel, which is being considered as the near-term fuel material for the SFR. The U-10Zr fuel material is comprised of 10 wt % zirconium and 90 wt % high-assay low-enriched U (HALEU) with an enrichment of approximately 16.5 wt %, and could attain a discharged burnup of up to 150 GWd/tHM. The ranges of enrichment and discharged burnup were in concordance with the SFR designs pursued by the industry (Neider 2021). The ABTR HALEU fuel was employed as the radiation source terms in the modeled accident scenarios as well.

Moreover, the spent nuclear fuel assembly derived from the PWR was also considered as the radiation source terms, specifically during the fuel reprocessing stage in scenarios 2 and 3. Notably, a fast reactor is commonly proposed to diminish the amount of spent nuclear fuel produced by the existing light-water reactor fleets by means of recycling the U and TRUs into a fuel. The spent fuel inventory of the PWR fuel was generated for a typical 3,000 MWth reactor whose fuel has an initial enrichment of 4.2 wt % and attains a burnup of 50 GWd/tHM (Kim and Taiwo 2010).

To determine the nuclide inventory of the ABTR irradiated fuel rapidly, ORIGEN reactor libraries were developed based on an ENDF/B-VII.1 nuclear data library (Chadwick et al. 2011) for ABTR U/TRU and HALEU fuels. This involved performing depletion calculations on a 2D axial slice of the core using

SCALE/TRITON to accurately capture the radial spectral effects. A softer neutron spectrum was observed in the outer fuel assemblies near the steel reflector region. However, the axial spectral effects on the one-group cross sections were determined to be negligible (Shaw et al. 2023). The resulting ABTR reactor libraries, generated using SCALE/TRITON, included parameterization of fuel burnup only because the one-group cross sections were found not to exhibit sensitivity to other irradiation parameters, such as temperature (Shaw et al. 2023). The generated ABTR reactor libraries covered burnup ranges up to 140 GWd/tHM for U/TRU fuels and 150 GWd/tHM for HALEU fuels, which exceeded the discharged burnup values. Meanwhile, the ORIGEN reactor libraries for a 17 × 17 PWR were used in SCALE/ORIGAMI to generate the nuclide inventory of the PWR spent fuel.

Figure 2 illustrates the fractional changes in the compositions between the fresh and the spent fuels for all the considered fuels. The ABTR spent fuels contained a higher proportion of TRUs and fission products (FPs) than the PWR's. For instance, the fractions of TRUs and FPs in the PWR spent fuel were only about 1.17 wt % and 4.55 wt %, respectively. On the other hand, the ABTR spent fuels contained more than 8 wt % of FPs and 6 wt % of TRUs, which was expected given that ABTR spent fuels are discharged at a higher burnup. Notably, the ABTR HALEU spent fuel had the highest fraction of FPs because of the highest burnup of ~150 GWd/tHM.

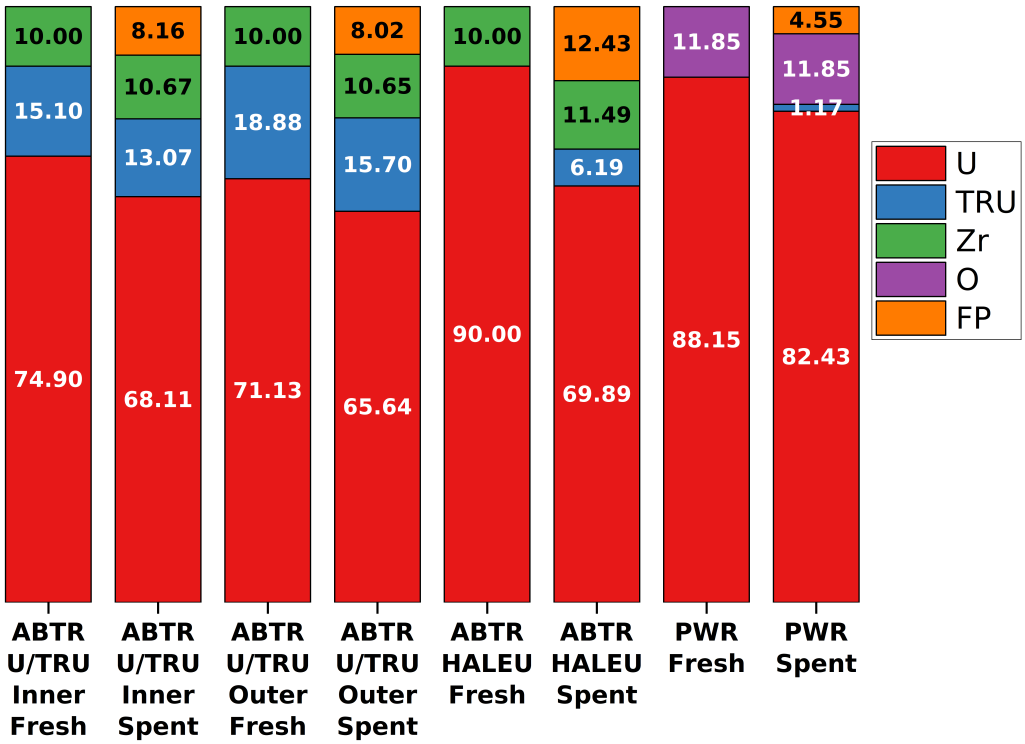

Figure 2. Composition distributions in the fresh and spent fuels (wt %).

Comparing the fractional changes in composition of the ABTR U/TRU and HALEU was also noteworthy. The ABTR HALEU spent fuel showed an approximate FP content of 12.43 wt %, which was significantly higher than that of the U/TRU spent fuel because of the former's higher burnup (~150 GWd/tHM). However, the TRU content in the ABTR HALEU spent fuel was only about 6.19 wt %, which was lower than that of the U/TRU fuel. This outcome was expected given that the ABTR U/TRU fuel is initially loaded with TRU.

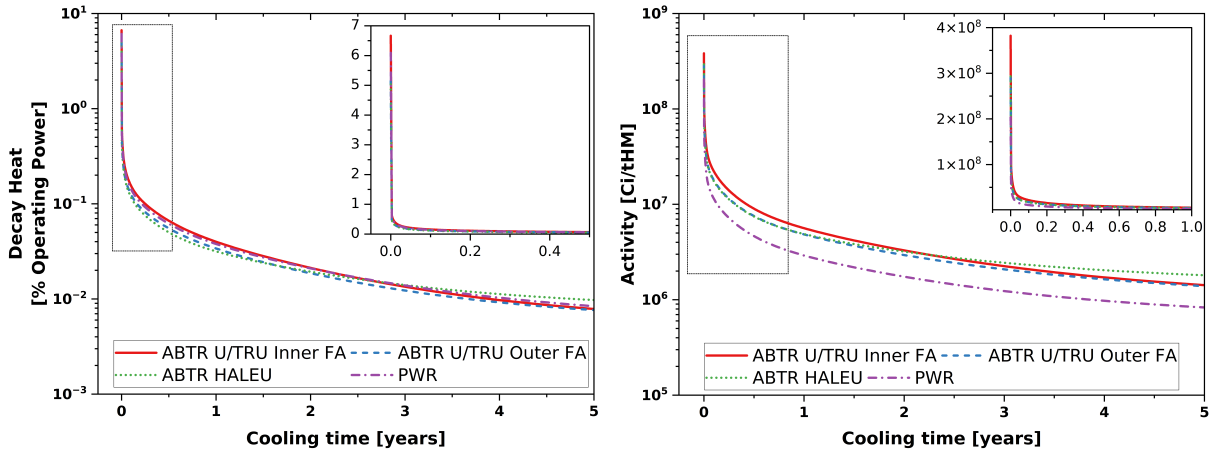

(a) Decay heat

(b) Activity

Figure 3. Decay heat and activity of the spent nuclear fuels.

Further analysis of decay heat and radionuclide activity showed important differences among these fuel assemblies. As depicted in Figure 3, the decay heat at shutdown accounted for approximately 5% to 7% of its operating power, with minimal variation among the considered spent fuel assemblies. The ABTR U/TRU inner fuel initially exhibited slightly higher decay heat due to its higher specific power, despite having lower burnup than the ABTR HALEU fuel. However, after approximately 3 years, the decay heat of the ABTR HALEU fuel may slightly exceed that of the other fuel assemblies due to its higher content of FPs. This observation was also reflected in the activity of the irradiated fuel after discharge. The activity of the ABTR HALEU was higher compared to the other fuel assemblies after approximately 3 years, consistent with the trend in decay heat. Moreover, the decay heat and activity of PWR spent fuel decreased faster than those of the ABTR because of the PWR spent fuel's lower FP buildup and fuel burnup. These findings provide a clear understanding of the characteristics of these spent nuclear fuels, which is vital for the physics of the analyses. The similarities observed in the characteristics of the inner and outer ABTR U/TRU fuels led to the inner fuel assembly being selected as the radiation source terms in this analysis.

4. ANALYSIS OF POSTULATED ACCIDENT SCENARIOS

4.1 RELEASE OF FISSION PRODUCTS DURING OPERATION/REFUELING

The ABTR fuel–handling system illustrated in Figure 4, which is situated within the containment building (CB), reloads the core with fresh fuel assemblies and removes fuel assemblies that have reached their ends of life out of the core. Fuel assemblies that have attained their target burnups are extracted from the core and transferred to an in-vessel storage rack located outside the reactor barrel, within the pool, for up to seven irradiation cycles. From there, the spent fuel assemblies are moved to an interbuilding cask pit. During this transfer, a seismic event was postulated, causing the refueling machine to collapse and to drop the fuel assembly inside the CB. Dose rates were evaluated for this ABTR postulated accident scenario for radiation sources from fuel assemblies at different cooling times, ranging from 10 days to the equivalent of 7 fuel irradiation cycles. The 10-day cooling time is associated with an off-normal event in which a spent fuel assembly with a much stronger radiation source is selected for extraction from the storage rack because of error.

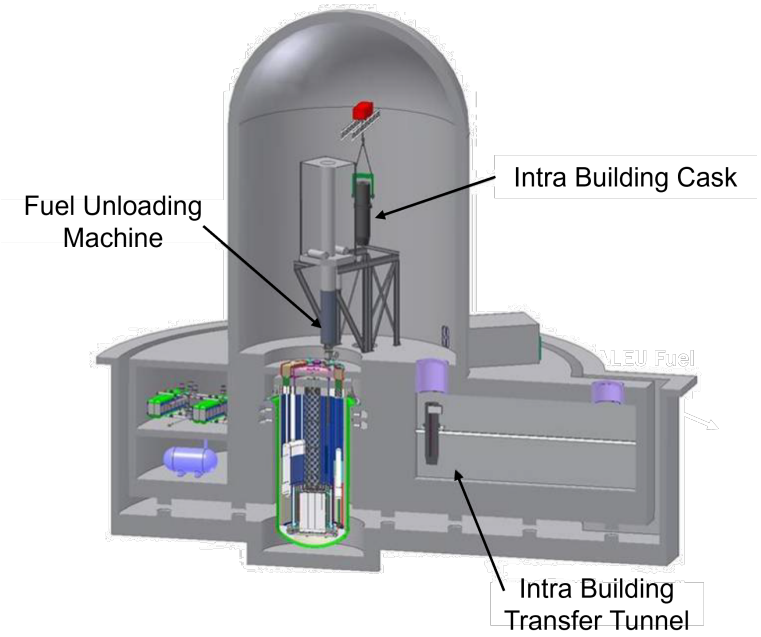

Figure 4. ABTR fuel–handling system (Chang, Finck, and Grandy 2006).

4.1.1 Radiation Source Term Characteristics

The calculated radiation source terms, including gamma and neutron sources in the fuel region and activation sources in the nonfuel regions, were characterized and are discussed. Gamma source intensity variation as a function of energy is shown in Figure 5 for the ABTR U/TRU and HALEU spent fuels with a 10-day cooling time and after the equivalent cooling period of 7 irradiation cycles (i.e., 840 days for U/TRU fuel and 3,780 days for HALEU fuel). The gamma source terms shown were generated on the 47–energy group structure available in SCALE, the energy values of which are provided in Table 2, along with group gamma intensity values. The U/TRU and HALEU spent fuels cooled for 10 days exhibited similar gamma source characteristics for gamma energies up to approximately 3.5 MeV. The gamma rays above 3.5 MeV were primarily the product of TRU nuclide decay. Therefore, the U/TRU gamma source intensity was significantly

higher than the HALEU gamma source intensity above 3.5 MeV, as shown in Figure 5, because U/TRU spent fuels have significantly greater TRU content than HALEU spent fuels (13.07 wt % vs. 6.19 wt %). However, the source intensity of gamma radiation with energy above 3.5 MeV was many orders of magnitude lower than the total gamma source intensity and is expected to make insignificant contributions to dose. The gamma source intensity of the U/TRU spent fuel was higher than that of the HALEU spent fuel after 7 irradiation cycles of cooling time because of difference cycle lengths (3,780 days for HALEU spent fuel compared to 840 days for U/TRU spent fuel, respectively, for 7 cycles).

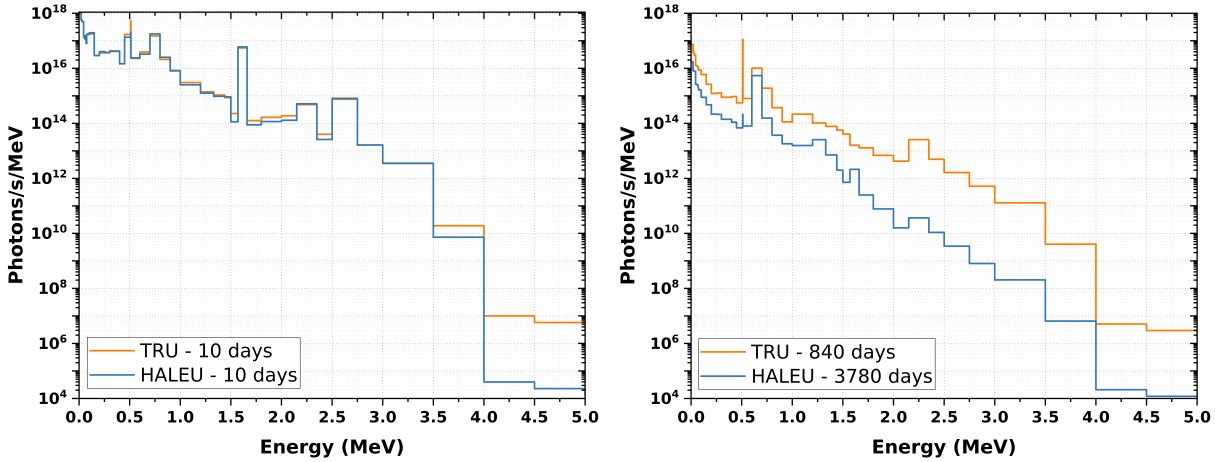

(a) Gamma source intensity at 10-day cooling

(b) Gamma source intensity at 7-cycle cooling

Figure 5. Gamma sources as a function of energy and cooling time for U/TRU and HALEU fuels.

Table 3 summarizes the FPs important to the gamma source terms; these FPs contributed more than 1% of the spent fuel assembly gamma sources within 0.4–3 MeV for each cooling time at the different spent fuel cooling times. Generally, gamma radiation within this energy range is expected to contribute significantly to the external dose rates of shielded spent fuel systems (US NRC 2020b). The FP nuclides are listed in Table 3 in order of increasing mass number. The contribution of a gamma-emitter nuclide to the dose rate is proportional to its nuclide activity and the energies and emission probabilities of its gamma rays. The FPs in Table 3 have been identified as gamma emitters in the ORIGEN output, but their individual contributions to the dose rate have not been determined in this study.

Many FPs contributed to the gamma source term of ABTR spent fuel cooled for only 10 days. The most important gamma emitter among these FPs was the short-lived ^{140}La ($T_{1/2}$ = 1.678 days), which is a direct FP and is also produced by ^{140}Ba ($T_{1/2}$ = 12.75 days) beta decay. Both FPs have large cumulative fast fission yields (e.g., approximately 6% for ^{235}U fission and 5.3% for ^{239}Pu fission), and the gamma emission spectrum of ^{140}La includes strong gamma rays (e.g., 2.522 and 1.597 MeV with emission probabilities of 3.4% and 95.4%, respectively). As seen in Figure 5, the gamma source term exhibited a peak at 1.597 MeV because of the higher intensity of the ^{140}La gamma rays.

The number of gamma emitters decreased with increasing cooling times due to their short half lives. Gamma emissions from ^{106}Rh, ^{154}Eu, ^{134}Cs, and ^{37m}Ba were important for longer cooling times. Beta particles from ^{90}Sr/^{90}Y have high endpoint energies (2.274 MeV) and produce high-energy bremsstrahlung radiation in spent fuel. Main Zr activation products that are gamma emitters include ^{95}Zr ($T_{1/2}$ = 64.02 days) and ^{95}Nb ($T_{1/2}$ = 34.99 days).

Table 2. Gamma source intensity (photons/s) as a function of energy

Energy Group	Energy group range (MeV)	U-TRU-10Zr		HALEU	
		10 days	840 days	10 days	3,780 days
1	$1.20 \times 10^{1} - 1.00 \times 10^{1}$	9.82×10^{3}	5.01×10^{3}	1.91×10^{2}	5.15×10^{1}
2	$1.00 \times 10^{1} - 8.00 \times 10^{0}$	1.34×10^{5}	6.85×10^{4}	2.62×10^{3}	7.09×10^{2}
3	$8.00 \times 10^{0} - 7.50 \times 10^{0}$	1.10×10^{5}	5.60×10^{4}	2.14×10^{3}	5.83×10^{2}
4	$7.50 \times 10^{0} - 7.00 \times 10^{0}$	1.89×10^{5}	9.65×10^{4}	3.70×10^{3}	1.01×10^{3}
5	$7.00 \times 10^{0} - 6.50 \times 10^{0}$	3.27×10^{5}	1.67×10^{5}	6.40×10^{3}	1.75×10^{3}
6	$6.50 \times 10^{0} - 6.00 \times 10^{0}$	5.63×10^{5}	2.87×10^{5}	1.11×10^{4}	3.03×10^{3}
7	$6.00 \times 10^{0} - 5.50 \times 10^{0}$	9.72×10^{5}	4.95×10^{5}	1.91×10^{4}	5.27×10^{3}
8	$5.50 \times 10^{0} - 5.00 \times 10^{0}$	1.68×10^{6}	8.55×10^{5}	3.31×10^{4}	9.15×10^{3}
9	$5.00 \times 10^{0} - 4.50 \times 10^{0}$	2.89×10^{6}	1.47×10^{6}	5.72×10^{4}	1.59×10^{4}
10	$4.50 \times 10^{0} - 4.00 \times 10^{0}$	4.99×10^{6}	2.54×10^{6}	9.90×10^{4}	2.77×10^{4}
11	$4.00 \times 10^{0} - 3.50 \times 10^{0}$	9.51×10^{9}	2.03×10^{9}	4.24×10^{9}	3.83×10^{6}
12	$3.50 \times 10^{0} - 3.00 \times 10^{0}$	1.79×10^{12}	6.47×10^{10}	1.24×10^{12}	1.18×10^{8}
13	$3.00 \times 10^{0} - 2.75 \times 10^{0}$	4.10×10^{12}	1.29×10^{11}	2.88×10^{12}	2.32×10^{8}
14	$2.75 \times 10^{0} - 2.50 \times 10^{0}$	1.87×10^{14}	4.05×10^{11}	1.38×10^{14}	1.41×10^{9}
15	$2.50 \times 10^{0} - 2.35 \times 10^{0}$	5.98×10^{12}	7.41×10^{11}	3.34×10^{12}	1.99×10^{9}
16	$2.35 \times 10^{0} - 2.15 \times 10^{0}$	9.60×10^{13}	5.10×10^{12}	7.33×10^{13}	6.77×10^{9}
17	$2.15 \times 10^{0} - 2.00 \times 10^{0}$	2.81×10^{13}	6.33×10^{11}	1.65×10^{13}	3.05×10^{9}
18	$2.00 \times 10^{0} - 1.80 \times 10^{0}$	3.29×10^{13}	1.37×10^{12}	1.95×10^{13}	2.07×10^{10}
19	$1.80 \times 10^{0} - 1.66 \times 10^{0}$	1.76×10^{13}	1.80×10^{12}	1.14×10^{13}	4.77×10^{10}
20	$1.66 \times 10^{0} - 1.57 \times 10^{0}$	4.96×10^{15}	1.44×10^{12}	3.67×10^{15}	3.96×10^{11}
21	$1.57 \times 10^{0} - 1.50 \times 10^{0}$	1.59×10^{13}	2.84×10^{12}	8.49×10^{12}	7.39×10^{10}
22	$1.50 \times 10^{0} - 1.44 \times 10^{0}$	5.15×10^{13}	3.40×10^{12}	4.20×10^{13}	2.17×10^{11}
23	$1.44 \times 10^{0} - 1.33 \times 10^{0}$	1.17×10^{14}	8.52×10^{12}	9.48×10^{13}	1.38×10^{12}
24	$1.33 \times 10^{0} - 1.20 \times 10^{0}$	1.80×10^{14}	1.34×10^{13}	1.70×10^{14}	7.25×10^{12}
25	$1.20 \times 10^{0} - 1.00 \times 10^{0}$	6.10×10^{14}	4.33×10^{13}	5.73×10^{14}	6.02×10^{12}
26	$1.00 \times 10^{0} - 9.00 \times 10^{-1}$	8.03×10^{14}	1.13×10^{13}	5.99×10^{14}	3.38×10^{12}
27	$9.00 \times 10^{-1} - 8.00 \times 10^{-1}$	2.09×10^{15}	3.70×10^{13}	2.04×10^{15}	6.70×10^{12}
28	$8.00 \times 10^{-1} - 7.00 \times 10^{-1}$	1.51×10^{16}	1.90×10^{14}	1.30×10^{16}	2.94×10^{13}
29	$7.00 \times 10^{-1} - 6.00 \times 10^{-1}$	3.92×10^{15}	1.02×10^{15}	3.59×10^{15}	8.21×10^{14}
30	$6.00 \times 10^{-1} - 5.12 \times 10^{-1}$	2.01×10^{15}	7.03×10^{13}	1.64×10^{15}	1.18×10^{13}
31	$5.12 \times 10^{-1} - 5.10 \times 10^{-1}$	1.05×10^{15}	2.24×10^{14}	4.79×10^{14}	5.13×10^{11}
32	$5.10 \times 10^{-1} - 4.50 \times 10^{-1}$	1.03×10^{16}	3.35×10^{13}	6.48×10^{15}	5.71×10^{12}
33	$4.50 \times 10^{-1} - 4.00 \times 10^{-1}$	7.37×10^{14}	4.73×10^{13}	5.41×10^{14}	7.40×10^{12}
34	$4.00 \times 10^{-1} - 3.00 \times 10^{-1}$	4.31×10^{15}	8.89×10^{13}	3.09×10^{15}	1.94×10^{13}
35	$3.00 \times 10^{-1} - 2.60 \times 10^{-1}$	1.47×10^{15}	5.09×10^{13}	1.15×10^{15}	1.17×10^{13}
36	$2.60 \times 10^{-1} - 2.00 \times 10^{-1}$	2.19×10^{15}	7.27×10^{13}	1.87×10^{15}	1.84×10^{13}
37	$2.00 \times 10^{-1} - 1.50 \times 10^{-1}$	1.44×10^{15}	1.30×10^{14}	1.14×10^{15}	3.26×10^{13}
38	$1.50 \times 10^{-1} - 1.00 \times 10^{-1}$	8.87×10^{15}	2.96×10^{14}	7.32×10^{15}	6.52×10^{13}
39	$1.00 \times 10^{-1} - 7.50 \times 10^{-2}$	4.18×10^{15}	2.15×10^{14}	3.28×10^{15}	5.79×10^{13}
40	$7.50 \times 10^{-2} - 7.00 \times 10^{-2}$	3.97×10^{14}	4.52×10^{13}	3.06×10^{14}	1.32×10^{13}
41	$7.00 \times 10^{-2} - 6.00 \times 10^{-2}$	1.12×10^{15}	1.15×10^{14}	8.88×10^{14}	3.43×10^{13}
42	$6.00 \times 10^{-2} - 4.50 \times 10^{-2}$	1.91×10^{15}	1.86×10^{14}	1.86×10^{15}	5.61×10^{13}
43	$4.50 \times 10^{-2} - 3.00 \times 10^{-2}$	7.26×10^{15}	4.55×10^{14}	5.52×10^{15}	1.69×10^{14}
44	$3.00 \times 10^{-2} - 2.00 \times 10^{-2}$	5.81×10^{15}	3.87×10^{14}	4.36×10^{15}	1.14×10^{14}
45	$2.00 \times 10^{-2} - 1.00 \times 10^{-2}$	9.69×10^{15}	7.36×10^{14}	8.16×10^{15}	2.39×10^{14}
	Total	9.09×10^{16}	4.49×10^{15}	7.22×10^{16}	1.73×10^{15}

Table 3. Nuclides important to gamma sources in spent U/TRU and HALEU fuels

10 days of cooling		7 cycles of cooling	
Nuclide	Half-life	Nuclide	Half-life
^{91}Y	58.5 days	^{90}Sr/^{90}Y	28.78 years/2.67 days
^{95}Zr	64.02 days	^{106}Ru/^{106}Rh	1.02 years/2.18 h
^{95}Nb	34.99 days	^{110m}Ag	249.8 days
^{103}Ru	39.27 days	^{125}Sb	2.758 years
^{106}Ru/^{106}Rh	1.02 years/2.18 h	^{134}Cs	2.065 years
^{124}Sb	60.2 days	^{137}Cs/^{137m}Ba	30.07 years/2.552 months
^{132}Te/^{132}I	3.2 days/2.28 h	^{144}Ce/^{144}Pr	284.6 days/17.28 months
^{134}Cs	2.065 years	^{152}Eu	13.54 years
^{136}Cs/^{136m}Ba	13.16 days/0.308 s	^{154}Eu	8.593 years
^{137}Cs/^{137m}Ba	30.07 years/2.552 months	—	—
^{140}Ba/^{140}La	12.75 days/1.678 days	—	—
^{144}Ce/^{144}Pr	284.6 days/17.28 months	—	—
^{147}Nd	10.98 days	—	—
^{148m}Pm	42.3 days	—	—
^{154}Eu	8.593 years	—	—
^{156}Eu	15.2 days	—	—

Meanwhile, the neutron sources were entirely produced by actinide spontaneous fission. Light-element impurities, which would contribute neutrons from (α,n) reactions, were not specified in the initial fuel compositions because no information is currently available about typical light-element impurity contents in these fuels. The main neutron emitters are presented in Table 4 along with their percentage contributions to the total fuel assembly neutron sources. For U/TRU spent fuel, the main neutron emitters were ^{244}Cm ($T_{1/2}$ = 18.10 years) and ^{242}Cm ($T_{1/2}$ = 162.8 days), with the latter having significant contributions only for the 10-day cooling time. The main neutron emitters in the HALEU spent fuel included ^{242}Cm and ^{240}Pu ($T_{1/2} = 6.56 \times 10^3$ years) at a 10-day cooling time and ^{240}Pu, ^{238}Pu ($T_{1/2}$ = 87.7 years), and ^{244}Cm at the longer cooling time. Neutron source intensity as a function of energy is illustrated in Figure 6 for the spent U/TRU and HALEU with the 10-day cooling time. The graph shows that the U/TRU spent fuel produced a greater neutron source than the HALEU spent fuel, primarily because of the initial high TRU content of the U/TRU fuel. The U/TRU spent fuel has 16.5% TRU initial content, which includes 50.8 g ^{244}Cm per tHM. However, the neutron sources were many orders of magnitude lower than the gamma sources and had negligible dose rate contributions for the cooling time range analyzed. For example, the maximum neutron dose rate was more than three orders of magnitude lower than the maximum gamma dose rate outside the CB, as seen in Section 4.1.2.

The nonfuel regions of the ABTR fuel assemblies, such as HT-9 alloy in cladding and ducts and stainless steel (SS) 316 alloy in the upper and lower structure regions, were also activated and taken into account in the radiation source terms calculation by SCALE/ORIGAMI. Six axial zones were used to consider the nonfuel regions because the neutron flux of nonfuel regions is much lower than that in the core (see the low scaling factor for the nonfuel regions in Table 5). The evaluated total neutron flux values for the calculated ratios of the nonfuel region flux to the fuel region flux for the upper plenum with a bond and the lower reflector were 31.7% and 37.1%, respectively, of the total neutron flux in the core region. Beyond these axial regions, the neutron flux decreased significantly, representing less than 10% of that of the fuel region flux. To account for the actual neutron flux in a nonfuel axial region, the activation source strength, determined as previously

Table 4. Relative contributions of key nuclides to neutron sources

Cooling time	ABTR HALEU	ABTR U/TRU
10 days	^{242}Cm (74.2%) ^{240}Pu (17.3%)	^{242}Cm (44.3%) ^{244}Cm (54.0%)
7 cycles	^{240}Pu (71.3%) ^{238}Pu (16.2%) ^{244}Cm (11.5%)	^{244}Cm (94.1%) ^{242}Cm (0.27%)

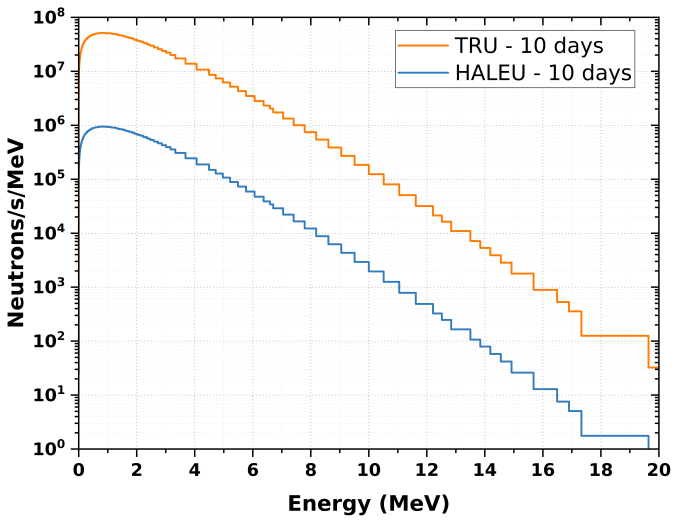

Figure 6. Neutron sources as a function of energy for U/TRU and HALEU spent fuels with a 10 day cooling time.

described, was multiplied by the ratio of the neutron flux of the nonfuel axial region to the fuel neutron flux. This ratio, denoted as the scaling factor in Table 5, was used to scale the activation source strength accordingly. Additionally, the fuel neutron spectrum was assumed for each of the nonfuel axial zones.

Table 5. Neutron flux in nonfuel materials

Axial zone	Nonfuel mixture	Total flux (n/cm^2s)	Scaling factor[a]
Lower structure	SS-316	5.0470×10^{13}	0.022
Lower reflector	HT-9	7.3475×10^{14}	0.317
Core	HT-9	2.3180×10^{15}	1.000
Upper plenum with Na bond	HT9	8.5988×10^{14}	0.371
Upper gas plenum	HT-9	1.9273×10^{14}	0.083
Upper structure	SS-316	4.6464×10^{13}	0.020
Duct	HT-9	1.0111×10^{15}	0.436

[a]Axial region neutron flux normalized to the core flux

The observed main activation products that are gamma emitters included ^{51}Cr ($T_{1/2}$ = 27.7 days), ^{59}Fe ($T_{1/2}$ = 44.5 days), ^{58}Co ($T_{1/2}$ = 70.85 days), ^{54}Mn ($T_{1/2}$ = 312.1 days), and ^{60}Co ($T_{1/2}$ = 5.272 years), which is an activation product of the Co impurity assumed in the alloy compositions. The evaluated activation gamma source was much lower than the FP gamma source, and consequently, the gamma dose rate produced by the activation products was negligible relative to the gamma dose rate produced by FP decay, as seen in Section 4.1.2.

4.1.2 Radiation Dose Rate

The computed dose rate values considered the contributions from previously discussed radiation source terms, which include gamma radiation emitted by unstable FPs, gamma radiation from the decay of activation products, Bremsstrahlung radiation, neutrons from spontaneous fission and subcritical multiplication, and secondary gamma radiation from neutron captures in materials. To calculate the dose, the 3D CB model was developed in SCALE/MAVRIC based on the ABTR design. It featured a cylindrical wall, which had an outer diameter of 19.639 m, a thickness of 98 cm, and a height of 17.942 m, closed by a hemispherical dome, which was 9.82 m high. The CB wall contained a 1.2 cm thick inner steel liner. The material composition of the reinforced concrete wall was based on a typical PWR reactor building rebar-to-concrete mass ratio for the reinforced concrete wall of 0.106 (Peterson, Zhao, and Petroski 2005).

ENDF/B-VII.1 continuous-energy cross sections (Chadwick et al. 2011) were used in the Monte Carlo calculations, and ANSI/ANS-1977 flux-to-dose-rate conversion factors (American Nuclear Society 1977) were applied to photon/neutron flux estimates. The dose rate inside the CB was calculated using a Cartesian mesh (dimensions x, y, z) subdivided into 20 × 20 × 20 cm voxels, and the dose rate outside the CB was calculated using a cylindrical mesh (dimensions r, θ, z) subdivided into 40 cm × 3° × 50 cm voxels. The relative statistical errors of the calculated dose rate values were less than 0.5% and 1% for the inner and outer regions of the CB, respectively.

A sensitivity study was performed to determine the fuel assembly location and orientation that results in the highest external dose rate. Two positions were analyzed, as depicted in Figure 7: (1) leaning on the CB wall and (2) lying on the floor next to the CB wall. The maximum inner dose rate value was not sensitive to the location of the fuel assembly analyzed (either on the floor or against the cylindrical wall). However, as seen in Figure 7, the fuel assembly leaning on the CB wall produced a greater maximum external dose rate by

approximately 10% than the other fuel location analyzed. Therefore, this model was used for all subsequent dose rate calculations.

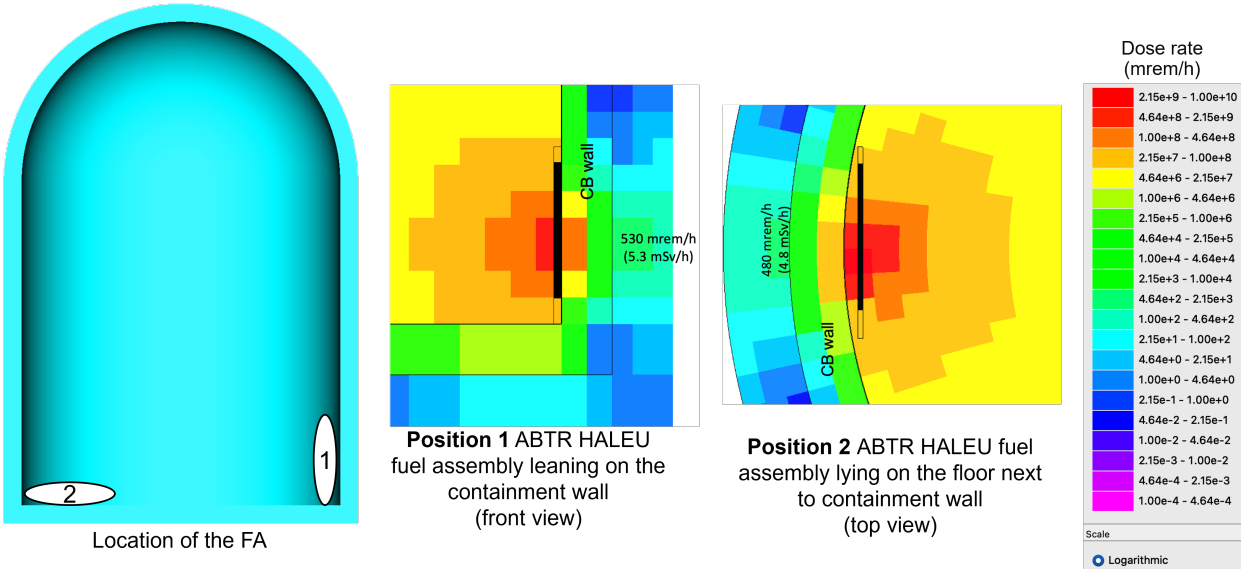

Figure 7. Sensitivity of external dose rate to fuel assembly (FA) location and orientation.

The dose rate maps for the inside and outside regions of the CB produced by the ABTR U/TRU and HALEU spent fuels with a 10-day cooling time are shown in Figure 8. Variations with spent fuel assembly cooling time of maximum dose rate values inside and outside the CB are shown on the graphs presented in Figure 9. The maximum dose rate values next to a fuel assembly with a 10-day cooling time were 1.31×10^4 Sv/h (1.31×10^6 rem/h) for the U/TRU spent fuel and 1.04×10^4 Sv/h (1.04×10^6 rem/h) for the HALEU spent fuel. These dose rate values are similar to the maximum dose rate of 1.7×10^4 Sv/h (1.7×10^6 rem/h) produced by an unshielded PWR fuel assembly with 0.467 MTU, an initial ^{235}U enrichment of 4.2%, a burnup value of 50 GWd/MTU, and a cooling time of 10 days.

The maximum external dose rate values produced by a spent fuel assembly considering all the radiation sources with a 10-day cooling time were 7.21 mSv/h (721 mrem/h) for the U/TRU fuel and 5.33 mSv/h (533 mrem/h) for the HALEU fuel. These maximum external dose rate values decreased by approximately two and three orders of magnitude for U/TRU spent fuel cooled for 840 days and HALEU spent fuel cooled for 3,780 days, respectively. In contrast, the dose rate maps produced by activation sources and neutrons in Figures 10 and 11 show that these radiation sources were negligible compared with FP gamma sources.

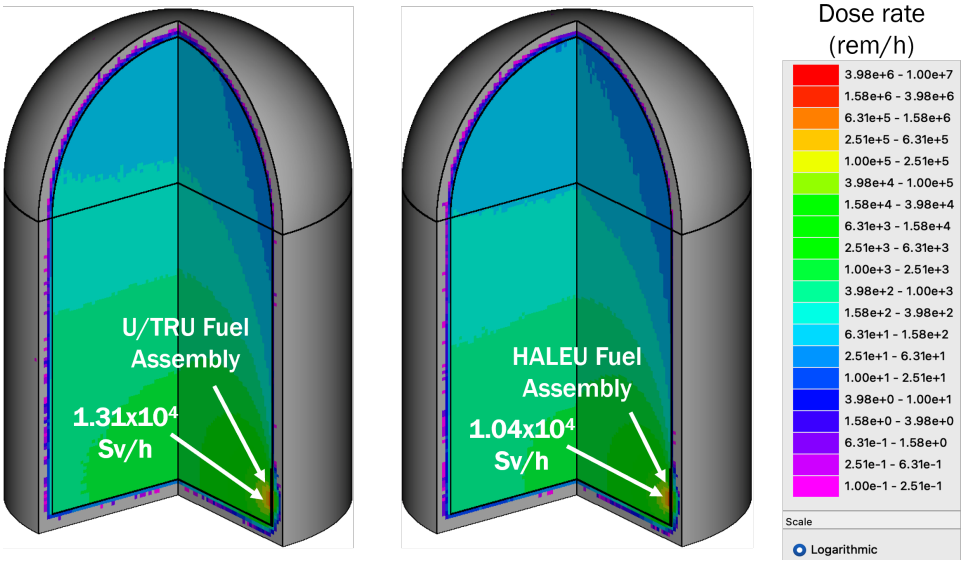

(a) Inside CB

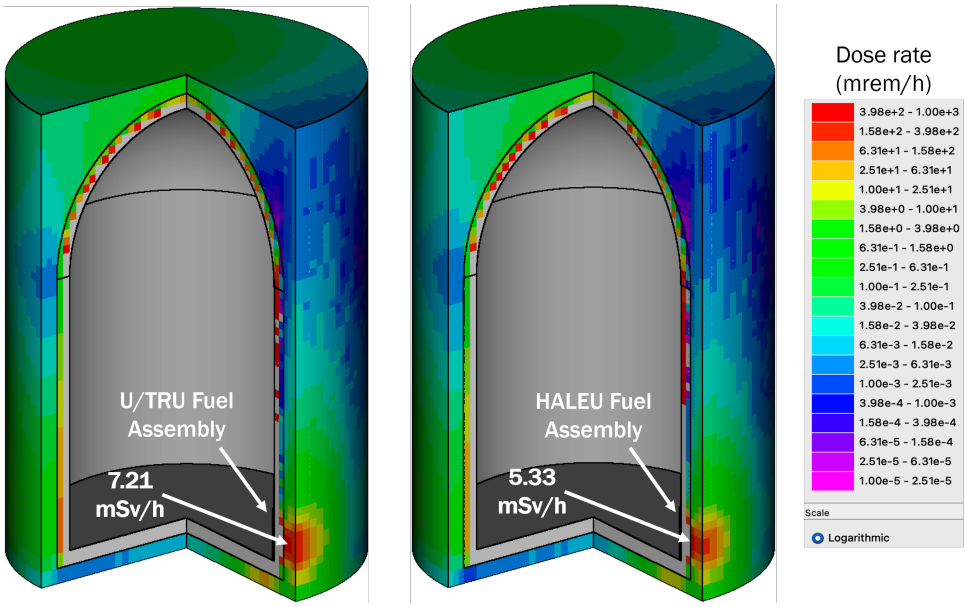

(b) Outside CB

Figure 8. Total dose rate maps inside and outside the CB at a 10-day cooling time.

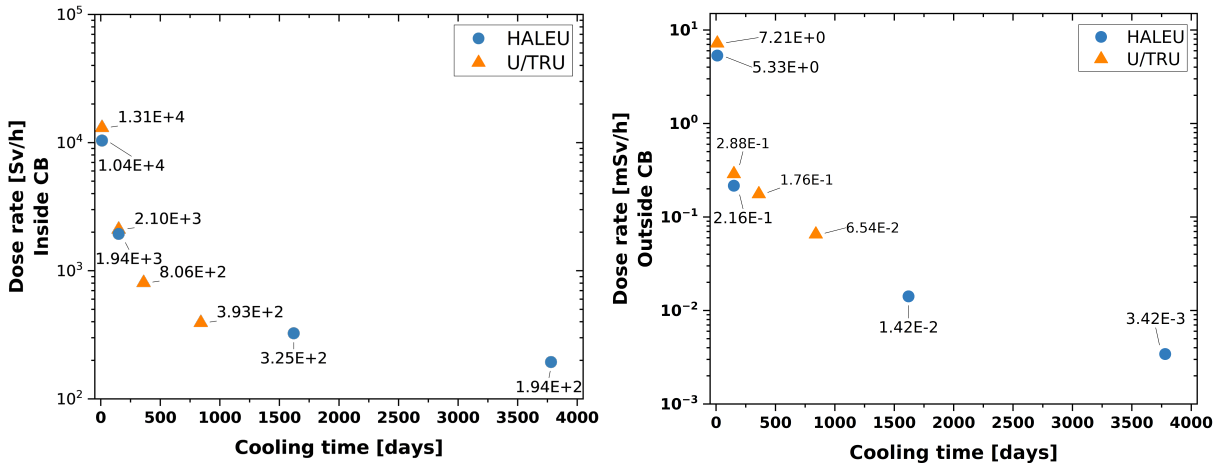

(a) Inside CB (b) Outside CB

Figure 9. Maximum dose rates inside and outside the CB as a function of cooling time.

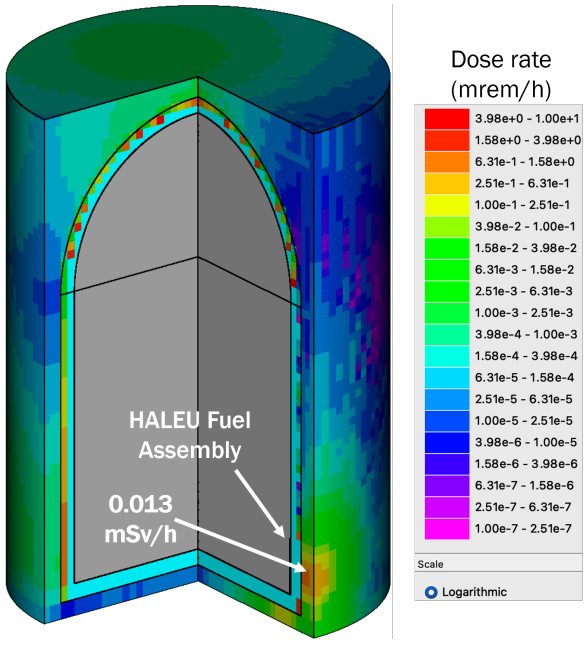

Figure 10. Dose rate map due to activation sources in HALEU spent fuel with a 10-day cooling time.

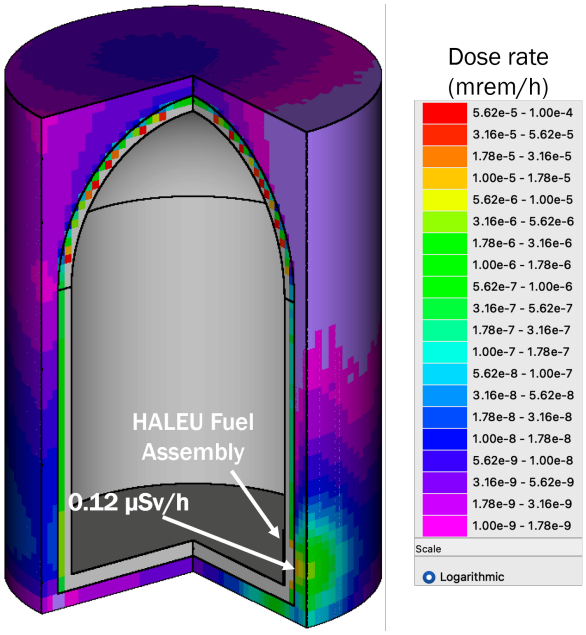

Figure 11. Dose rate map due to neutron sources in HALEU spent fuel with a 10-day cooling time.

It is worth mentioning that the occupational annual dose limit for adults in Title 10 of the Code of Federal Regulations, Part 20.1201, specifies a total effective dose equivalent of 5,000 mrem (50 mSv). Although the presence of personnel at locations near the CB exterior wall is not expected, the postulated accident scenario would cause a significant increase in the effective dose equivalent for external exposures only if a spent fuel assembly cooled for 10 days were inadvertently selected for transfer.

4.2 CRITICALITY EVENT/FISSILE MATERIAL BUILDUP DURING REPROCESSING

The electrometallurgical processing technology was proposed by ANL to address the treatment of all US Department of Energy spent fuels (National Research Council 2000; Fredrickson et al. 2022). Although reprocessing of nuclear fuel is not currently implemented in the United States, it is covered in this work as a basis for code demonstration for closed fuel cycles. In nuclear energy systems, fuel cycles can be categorized as either open or closed. In an open fuel cycle, nuclear fuel is used once in a reactor and then considered spent, with the spent fuel typically treated as waste and stored in repositories without reprocessing. Conversely, in a closed fuel cycle, spent nuclear fuel is reprocessed to extract useful materials such as uranium and plutonium. These materials can then be recycled and reused as fuel in reactors, allowing for additional energy extraction and reducing the volume and radiotoxicity of nuclear waste.

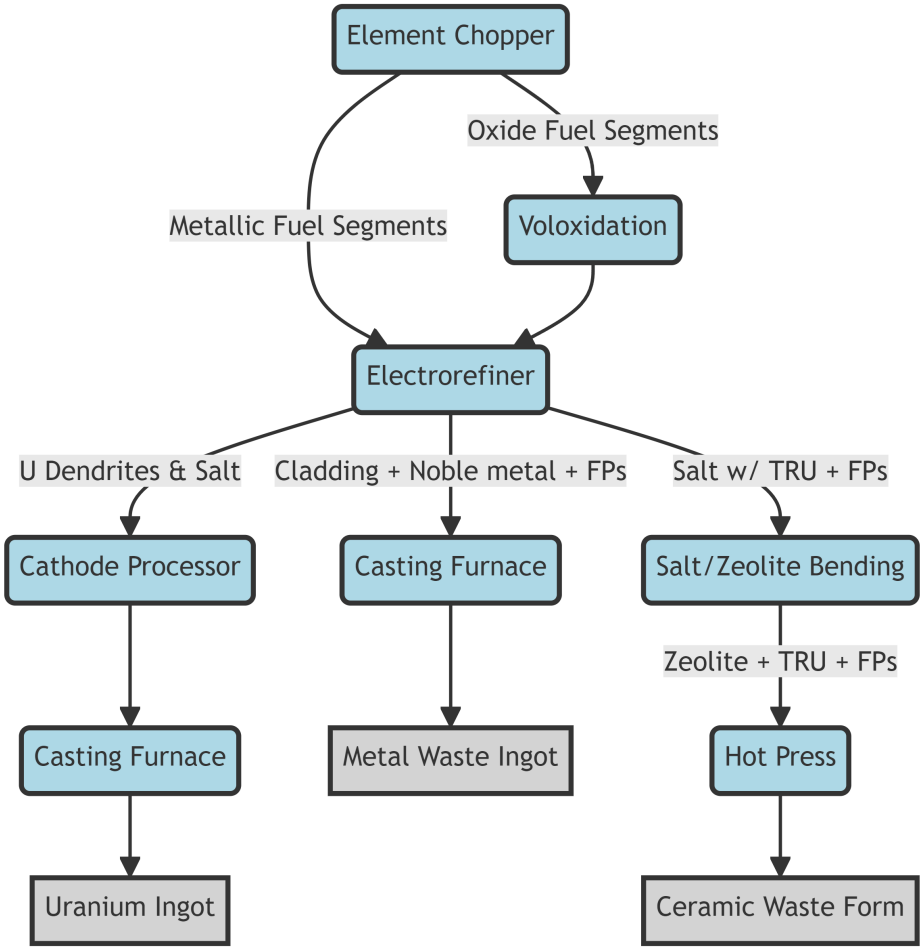

Figure 12. Electrometallurgical processing diagram (National Research Council 2000).

The present study builds upon the insights from treating spent nuclear fuel in Experimental Breeder Reactor II (EBR-II), as illustrated in Figure 12. The fuel assembly is chopped initially, and the resulting fuel segments are put into an electrorefiner. This process yields pure U salt, which can undergo further processing to become the final product (e.g. uranium metal ingot). TRUs, along with some FPs, become dissolved in the salt and treated as waste. An additional process is necessary for recycling UO_2 spent fuel, for example, originating from PWRs. In this case, the oxide fuel segments undergo oxide reduction (voloxidation) producing U_3O_8 before being transferred into the electrorefiner.

3D SCALE/CSAS-Shift electrorefiner models for criticality calculations were developed based on publicly available information and included many assumptions because of a lack of data specifically related to waste salt compositions. A 40-inch diameter and 40-inch height electrorefiner was modeled with single and dual cathodes as illustrated in Figure 13 (Mariani et al. 1996). The anode basket, containing the chopped fuel segments, was represented as a hollow cylindrical region containing salt. At the bottom of the electrorefiner, there was a cadmium pool, 6 inches deep, followed by a 12-inch-thick layer of molten salt. The cadmium pool was included to gather fallen uranium dendrites from the cathode (Li 2008).

Initially, molten LiCl-KCl eutectic at 500°C was used as the salt. However, as spent fuel is processed, the TRUs and FPs accumulate in the salt. In this study, the salt was assumed to be loaded with 10 wt % of TRUs and FPs. The FPs dissolved in the salt were the elements from alkali metal, alkali earth, rare earth, and noble

metals (Laidler et al. 1997). The complex geometry of the U dendrite collected in the steel cathode was defined as a homogeneous mixture because such complexity was impractical to handle with SCALE/CSAS's geometry packages. It is also important to note that simplifying the dendrite's geometry to a homogeneous mixture may not significantly impact the resulting k_{eff}. The steel cathode in the homogeneous U region had a radius of 3.175 cm and a length of 17.48 cm, and the outer diameter and the height of the U region were 25.4 cm.

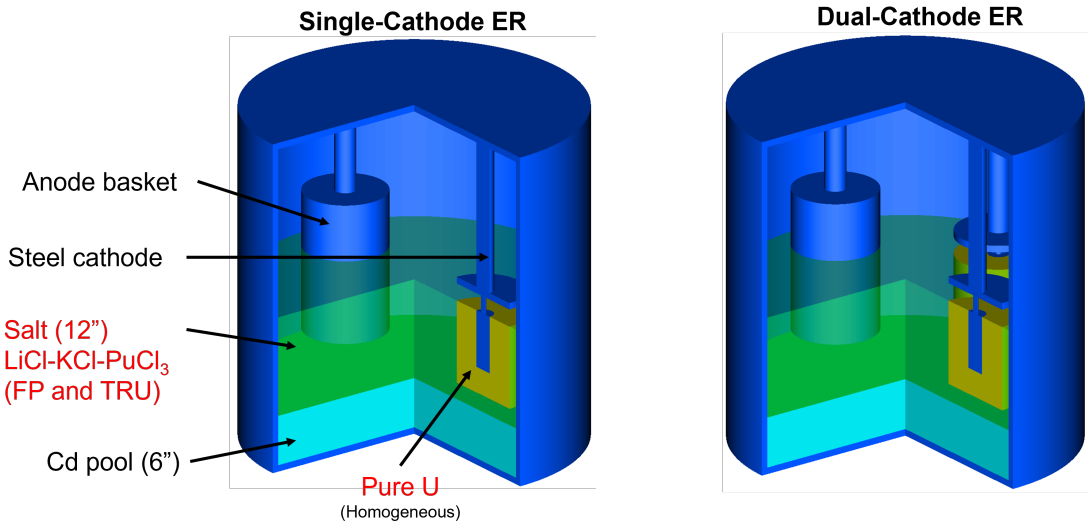

Figure 13. SCALE electrorefiner (ER) models.

Four configurations were studied for both the single- and the dual-cathode electrorefiners:

1. Electrorefiner with vacuum boundary conditions to simulate a single eletrorefiner (Figure 13),
2. Electrorefiner with reflective boundary conditions to simulate an array of electrorefiners (Figure 13),
3. Electrorefiner positioned in the center of a concrete room, surrounded by air (Figure 14),
4. Electrorefiner positioned in the center of a flooded concrete room (Figure 14).

The electrofiners were loaded with 3 different recycled fuels:

1. ABTR U/TRU spent fuel with burnup of 94.5 GWd/tHM and after 5 years of cooling,
2. ABTR HALEU spent fuel with burnup of 149.74 GWd/tHM and after 5 years of cooling,
3. PWR spent fuel with burnup of 50 GWd/tHM and after 10 years of cooling.

For all 24 models (2 electrofiner models $\times$ 4 configurations $\times$ 3 fuel types), the following criticality calculations were performed:

1. Criticality as a function of the U mass building up in the steel cathode. The U mass in the cathode was varied using a density multiplier ranging from 0.1 to 1.0 while assuming a U theoretical density of 18.56 g/cm^3,
2. Criticality as a function of the salt height in the electrorefiner while considering the maximum mass of U in the steel cathode.

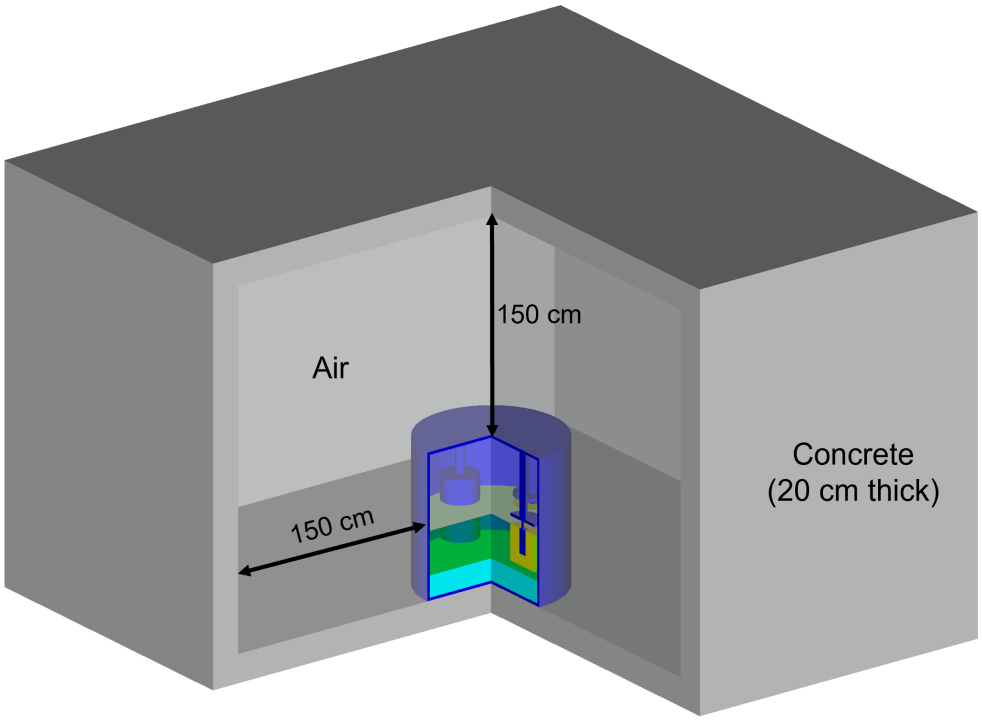

Figure 14. SCALE model of a electrorefiner (ER) placed in a room .

Figures 15 and 16 present the multiplication factor (k) of for the first two electrorefiner configurations, i.e. the single electrorefiner with vacuum and with reflective boundary conditions, as a function of U mass in the cathode and as a function of the salt height, respectively. The analyses were performed using both ENDF/B-VII.1 (Chadwick et al. 2011) and ENDF/B-VIII.0 (Brown et al. 2018) continuous-energy libraries. The application of reflective boundary conditions allows the assessment of the infinite multiplication factor (k_{inf}) for an infinite array of electrorefiners in both axial and radial directions, while the vacuum boundary condition defines a single, isolated bare electrorefiner, resulting in the evaluation of the effective multiplication factor (k_{eff}).

For the isolated bare electrorefiner, k_{eff} consistently remained lower than the typical limit of 0.95 for criticality safety, even at the maximum conditions for the U mass in the cathode and the increased salt height. The same is valid for the reflected electrorefiner model when using HALEU and PWR spent fuel. However, when varying the salt height, the reflected electrorefiner model with ABTR U/TRU spent fuel resulted in k_{inf} exceeding the safety limit of 0.95 when the additional salt height surpassed 70%.

The increase in k with U mass in the cathode when recycling HALEU spent fuel is due to the fact that the ABTR HALEU spent fuel still contained approximately 6% ^{235}U. Increasing the U mass in the cathode consequently leads to more fissile material in the cathode and a k increase. A similar, but less steep, increase is observed for the same reason when recycling PWR spent fuel and increasing the U mass in the cathode. Because the remaining fissile material in the ABTR U/TRU spent fuel is Pu which is present at a high weight fraction of approximately 68% in the salt, the multiplication factor for recycled U/TRU fuel is steeply increasing with an increasing salt height in the tank. However, due to a small fraction of ^{235}U (0.08%) and a high fraction of ^{238}U (99.88%) of the U in the cathode, k is only insignificantly impacted by an increased U mass in the cathode in a single electrorefiner configuration. Furthermore, in an array of electrorefiners configuration, k exhibits a gradual decrease with an increasing U mass due to increasing absorption rate by ^{238}U.

Consistent k results were found for both applied nuclear data libraries with overall absolute maximum k differences of 197 ± 9 pcm. Additionally, a negligible increment in k was observed between the single- and the dual-cathode models.

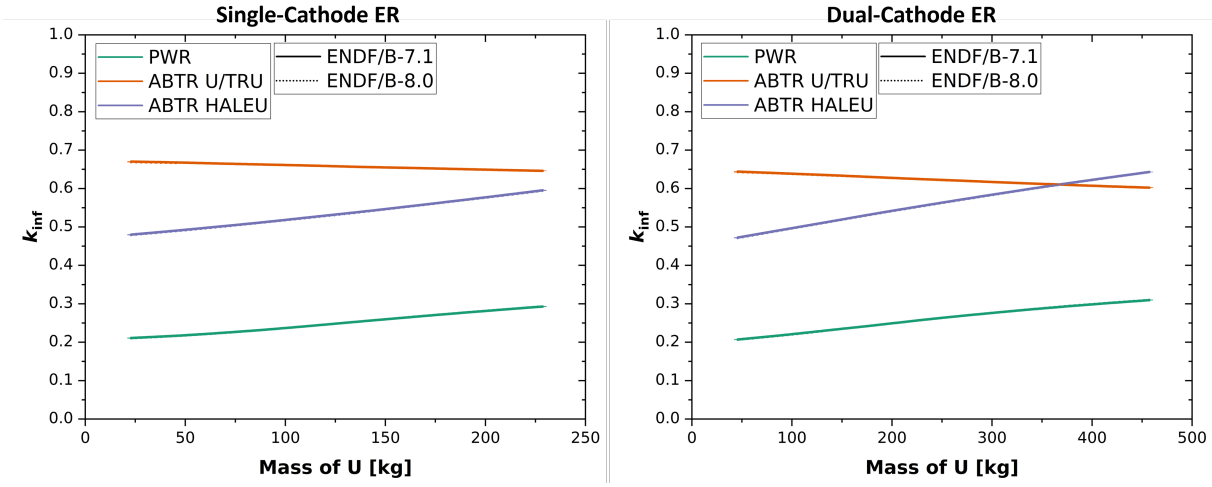

(a) With reflective boundary conditions

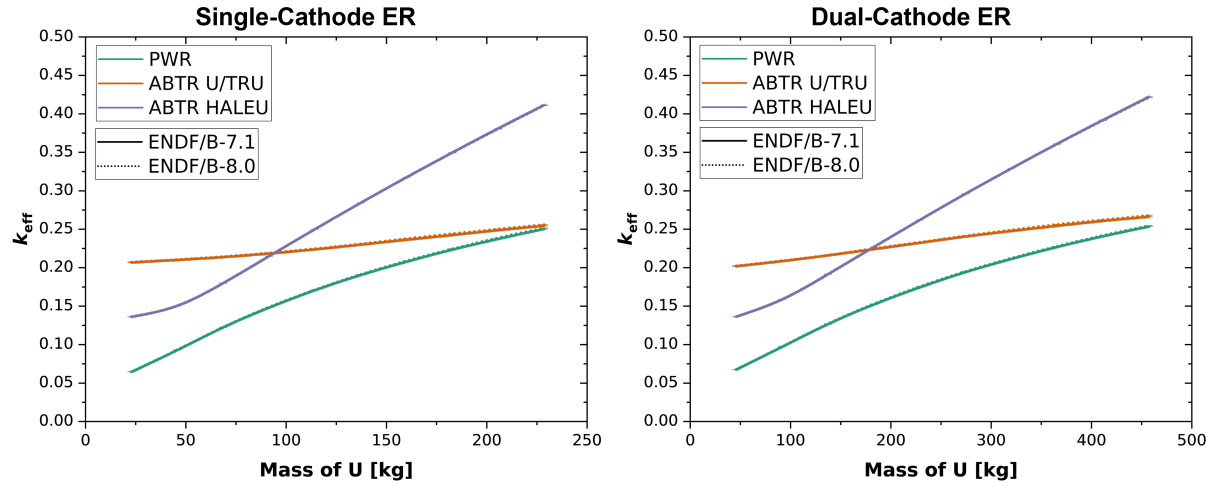

(b) With vacuum boundary conditions

Figure 15. Multiplication factor of a bare electrorefiner as a function of U mass in the cathode.

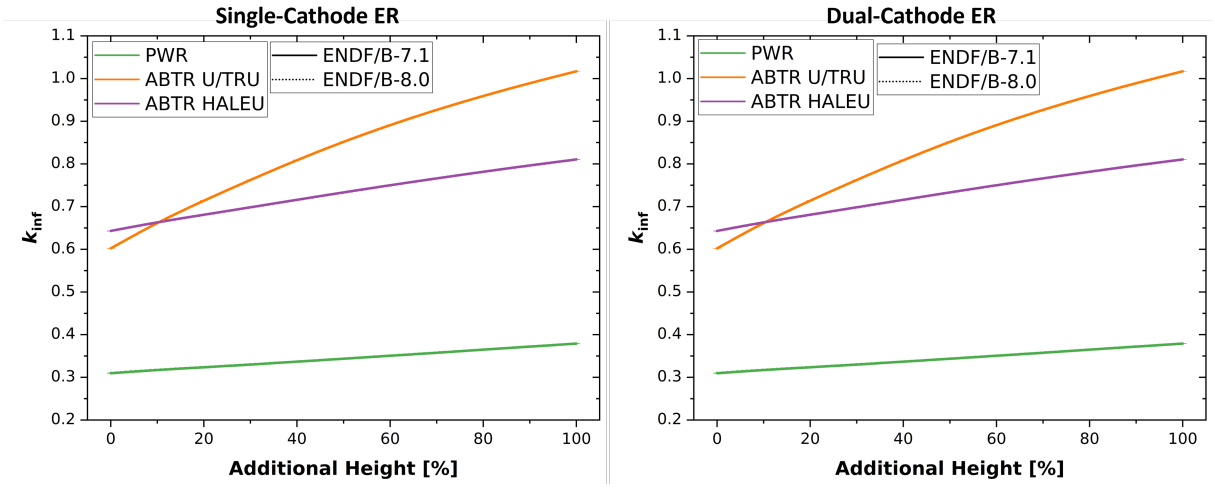

(a) With reflective boundary conditions

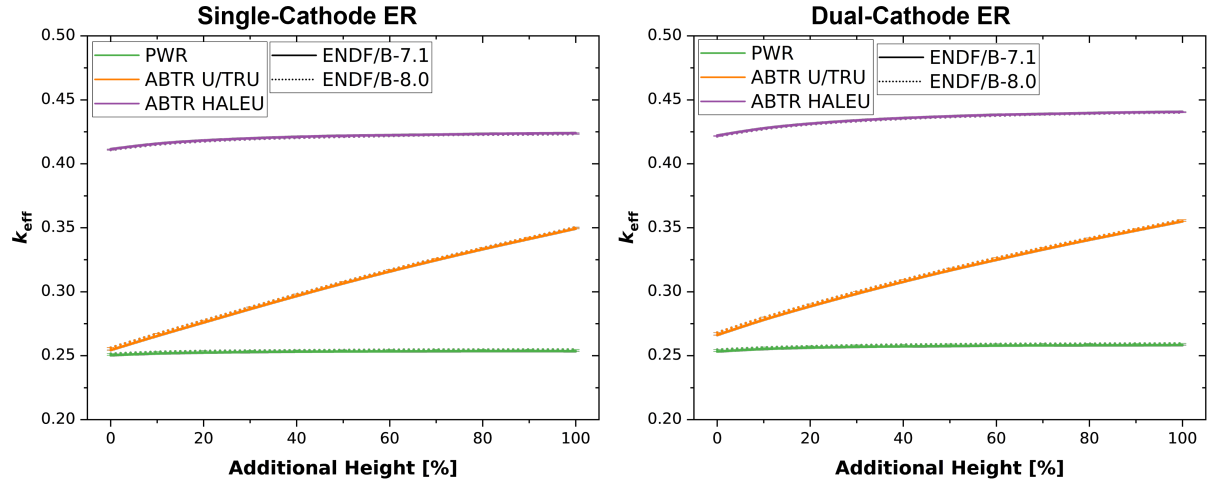

(b) With vacuum boundary conditions

Figure 16. Multiplication factor of a bare electrorefiner as a function of salt height in the tank.

Figures 17 and 18 provide the k_{eff} of the electrorefiner model located in the center of a room at normal and flooded conditions. In the flooded conditions, the air within the room was replaced by water to represent increased neutron moderation. The results show that the k_{eff} trend at normal conditions aligns with the bare electrorefiner model employing the vacuum boundary conditions. In all cases, including the flooded conditions, k_{eff} remained below the subcriticality safety limit of 0.95. The maximum k_{eff} increase of approximately 5243 ± 14 pcm due to flooding was found for the maximum salt height when recycling ABTR U/TRU spent fuel. Similar to the previous analysis of the bare electrorefiner, the higher increase in k_{eff} during the flooded condition when recycling ABTR U/TRU spent fuel is attributed to the higher fraction of plutonium in the salt. A minimal increase of k_{eff} between the results of ENDF/B-VII.1 and ENDF/B-VIII.0 (maximum 226 ± 19 pcm) was observed for all cases. On the other hand, the maximum difference in k_{eff} between single- and dual-cathode electrorefiners was about 2012 ± 16 pcm for all cases.

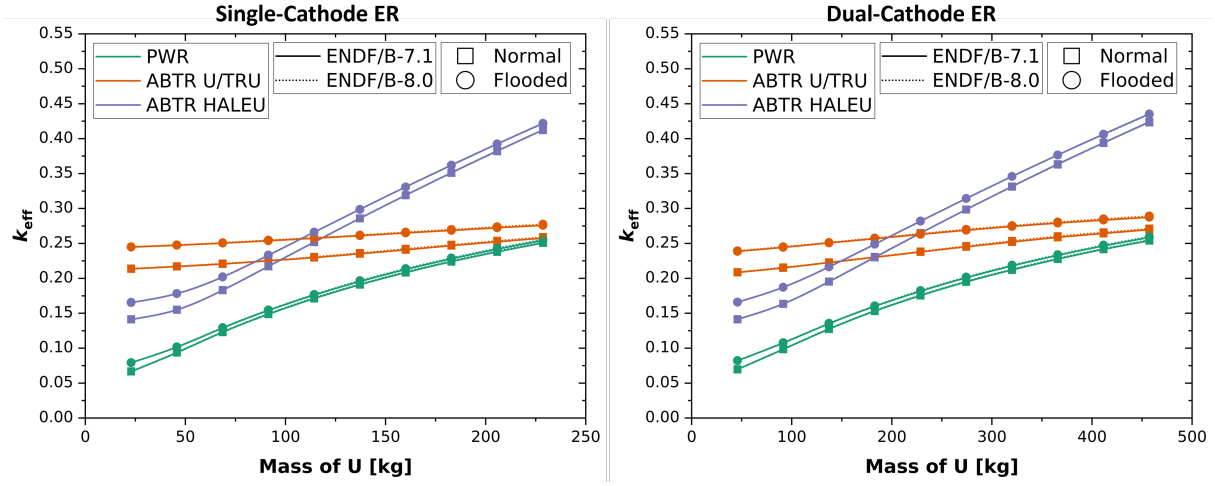

Figure 17. Multiplication factor of an electrorefiner placed in the center of a room as a function of U mass in the cathode.

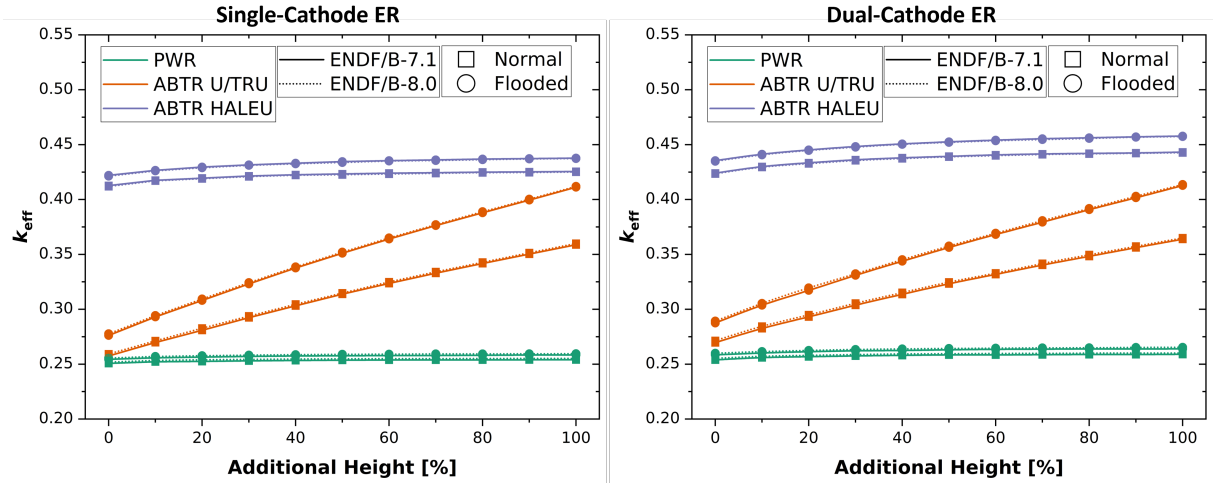

Figure 18. Multiplication factor of an electrorefiner placed in the center of a room as a function of salt height in the tank.

4.3 RELEASE OF FISSION PRODUCTS DURING REPROCESSING

One of the waste streams during the reprocessing stage is the gaseous and volatile FPs, including I, Xe, and Kr, typically collected during the fuel chopping stage. These FPs can be retained in a tank and safely released to the environment directly once their activities decay to low enough values. Figure 19 depicts the activity of these gaseous and volatile FPs, measured in Ci/metric ton heavy metal (MTHM), for the three recycled spent fuels. Notably, the salt recycling ABTR HALEU spent fuel had the highest activity because it contained more gaseous and volatile FPs due to higher burnup.

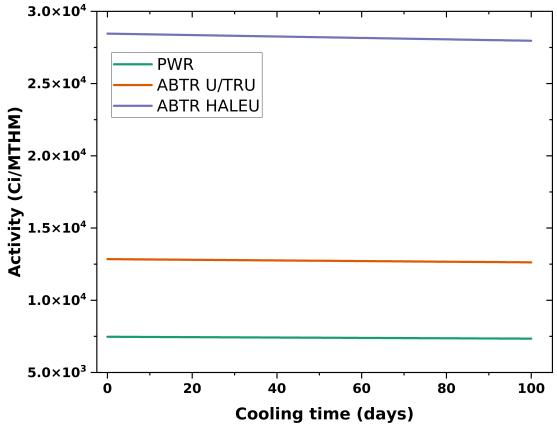

Figure 19. Activity of the gaseous and volatile fission products as a function of decay time.

Another waste stream during the reprocessing stage is the used salt that contains TRUs and FPs. In this scenario, the used salt storage tank was assumed to leak. The volumetric activity of the salt used in Section 4.2 was calculated as a function of cooling time and is illustrated in Figure 20. Similar to Figure 19, the salt recycling ABTR HALEU spent fuel had the highest activity because it contained more FPs. The activity of the salt was about 4.6 Ci/ml. According to the International Atomic Energy Agency (1972), liquid-waste activity larger than 10^{-2} Ci/ml requires cooling and shielding. However, the obtained activity in this study should be further confirmed because many assumptions were used to obtain the salt composition because of a lack of publicly available information. This analysis considered all TRUs and the majority of the FPs dissolved in the salt, but future studies should aim to refine these assumptions for more accurate assessments.

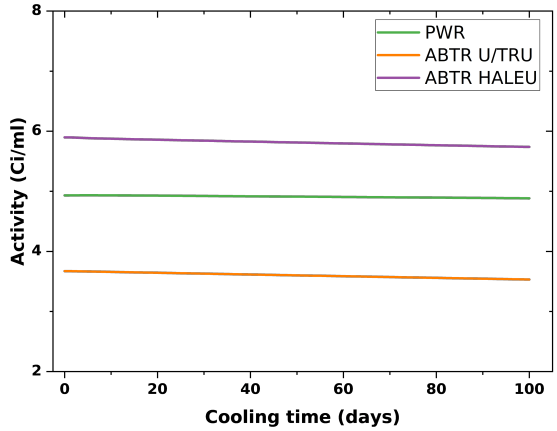

Figure 20. Volumetric activity of the salt as a function of decay time.

5. CONCLUSIONS

The presented study showcased SCALE 6.3.1 capabilities in analyzing postulated accident scenarios across different stages of the SFR nuclear fuel cycle, in support of the NRC non-LWR fuel cycle demonstration project. Three distinct accident scenarios were investigated, selected based on their suitability for code demonstration, regardless of their probability of occurrence. Utilizing the ABTR as the SFR reference design, the analyses covered both ABTR U/TRU-10Zr fuel and U-10Zr metallic fuel, reflecting recent industry design choices.

In the first scenario, a seismic event was assumed, resulting in the collapse of the refueling machine, and releasing a spent fuel assembly inside the reactor CB. Radiation source terms were generated for a cooling time of 10 days and the equivalent of 7 irradiation cycles, and the dose rates from radiation exposures inside and outside the CB were calculated. The radiation source terms generated with SCALE/ORIGAMI showed that gamma radiation dominated ABTR radiation sources and dose rates. The dose rate at 10 days of cooling produced by the ABTR spent fuel, whether U/TRU or HALEU, was similar to that produced by a representative PWR spent fuel with a burnup of 50 GWd/MTU. However, validation through assay measurements is essential to confirm the accuracy of the SCALE's predicted radiation source terms.

A criticality analysis of the electrorefiner was conducted in the second scenario. Using limited publicly available information, a SCALE/CSAS electrorefiner model was developed and multiple configurations were analyzed. The effective multiplication factor of all single electrorefiner models was found lower than the subcriticality limit of 0.95 in all considered configurations, including the variations of U mass in the steel cathode, the height of the salt, the number of steel cathodes, and during the flooded conditions. Only for a specific configuration of a reflected model that simulates a lattice of electrorefiners, when recycling U/TRU and when largely increasing the salt height in the tank, a multiplication factor larger than 0.95 was obtained. Consistent results were obtained when using the ENDF/B-VII.1 and ENDF/B-VIII.0 nuclear data libraries, with a maximum obtained difference of 226 ± 19 pcm.

The activity of the gaseous and volatile FPs and the volumetric activity of liquid salt that contains TRUs and FPs were evaluated in the third scenario. The findings emphasized the necessity of shielding and cooling measures for the liquid salt. However, assumptions were made regarding salt mixtures, presuming the inclusion of all TRUs and the majority of FPs. For future analyses to obtain accurate results, detailed information on the salt compositions during reprocessing is indispensable.

Overall, this study effectively demonstrated the diverse capabilities of the SCALE code system, including inventory generation, criticality, and shielding analyses of the SFR nuclear fuel cycle through the three selected scenarios. As additional details regarding configurations, dimensions, and compositions become available across various stages of the SFR nuclear fuel cycle, further analyses can be conducted to enhance result accuracy. To improve the generation of accurate fuel inventory at all times during SFR operation, a new capability in SCALE is proposed that calculates SFR equilibrium cycles. Additionally, incorporating a capability to model complex geometries, including the dendritic shape of U in the steel cathode during reprocessing, by allowing users to provide a geometry defined through an unstructured mesh would enhance modeling accuracy.

6. REFERENCES

American Nuclear Society. 1977. *ANSI/ANS 6.1.1-1977, American National Standard Neutron and Gamma-Ray Flux-to-Dose-Rate Factors.* La Grange Park, IL: American Nuclear Society.

Bostelmann, F., C. Celik, R. F. Kile, and W. A. Wieselquist. 2022. *SCALE Analysis of a Fluoride Salt-Cooled High-Temperature Reactor in Support of Severe Accident Analysis.* Technical report ORNL/TM-2021/2273. Oak Ridge, TN: Oak Ridge National Laboratory. https://doi.org/10.2172/1854475.

Bostelmann, F., E. E. Davidson, W. A. Wieselquist, D. Luxat, K. C. Wagner, and L. I. Albright. 2023. *Non-LWR Fuel Cycle Scenarios for SCALE and MELCOR Modeling Capability Demonstration.* Technical report ORNL/TM-2023/2954. Oak Ridge, TN: Oak Ridge National Laboratory. https://doi.org/10.2172/2251628.

Brown, D.A., M.B. Chadwick, R. Capote, A.C. Kahler, A. Trkov, M.W. Herman, A.A. Sonzogni, et al. 2018. "ENDF/B-VIII.0: The 8th Major Release of the Nuclear Reaction Data Library with CIELO-project Cross Sections, New Standards and Thermal Scattering Data." *Nuclear Data Sheets* 148:1–142. https://doi.org/10.1016/j.nds.2018.02.001.

Chadwick, M.B., M. Herman, P. Obložinský, M.E. Dunn, Y. Danon, A.C. Kahler, D.L. Smith, et al. 2011. "ENDF/B-VII.1 Nuclear Data for Science and Technology: Cross Sections, Covariances, Fission Product Yields and Decay Data." *Nuclear Data Sheets* 112 (12): 2887–2996. https://doi.org/10.1016/j.nds.2011.11.002.

Chang, Y. I., P. J. Finck, and C. Grandy. 2006. *Advanced Burner Test Reactor Preconceptual Design Report.* Technical report ANL-ABR-1 (ANL-AFCI 173). Argonne, IL: Argonne National Laboratory. https://doi.org/10.2172/946035.

Evans, T. M., A. S. Stafford, R. N. Slaybaugh, and K. T. Clarno. 2010. "Denovo: A New Three-Dimensional Parallel Discrete Ordinates Code in SCALE." *Nuclear Technology* 171 (2): 171–200. https://doi.org/10.13182/NT171-171.

Fredrickson, G. L., M. N. Patterson, D. Vaden, G. G. Galbreth, T.-S. Yoo, J. C. Price, E. J. Flynn, and R. N. Searle. 2022. "History and Status of Spent Fuel Treatment at the INL Fuel Conditioning Facility." *Progress in Nuclear Energy* 143:104037. https://doi.org/10.1016/j.pnucene.2021.104037.

Humphries, L. L., B. A. Beeny, F. Gelbard, D. L. Louie, J. Phillips, R. C. Schmidt, and N. E. Bixler. 2021. *MELCOR Computer Code Manuals - Vol. 1: Primer and Users' Guide Version 2.2.18019.* Technical report SAND2021-0726 O. Albuquerque, NM: Sandia National Laboratories.

International Atomic Energy Agency. 1972. *Storage Tanks for Liquid Radioactive Wastes.* Technical Reports Series 135. Vienna: International Atomic Energy Agency. https://www.iaea.org/publications/1236/storage-tanks-for-liquid-radioactive-wastes.

Kim, T. K. 2020. *Benchmark Specification of Advanced Burner Test Reactor.* Technical report ANL-NSE-20/65. Argonne, IL: Argonne National Laboratory. https://doi.org/10.2172/1761066.

Kim, T. K., and T. A. Taiwo. 2010. *Fuel Cycle Analysis of Once-Through Nuclear Systems.* Technical report ANL-FCRD-308. Argonne, IL: Argonne National Laboratories. https://doi.org/10.2172/989083.

Laidler, J. J., J. E. Battles, W. E. Miller, J. P. Ackerman, and E. L. Carls. 1997. "Development of Pyroprocessing Technology." *Progress in Nuclear Energy* 31 (1): 131–140. https://doi.org/10.1016/0149-1970(96)00007-8.

Li, Shelly X. 2008. "Experimental Observations on the Roles of the Cadmium Pool in the Mark-IV Electrorefiner." *Nuclear Technology* 162 (2): 144–152. https://doi.org/10.13182/NT08-A3941.

Lo, A., F. Bostelmann, D. Hartanto, B. Betzler, and W. A. Wieselquist. 2022. *Application of SCALE to Molten Salt Fueled Reactor Physics in Support of Severe Accident Analyses.* Technical report ORNL/TM-2022/1844. Oak Ridge, TN: Oak Ridge National Laboratory. https://doi.org/10.2172/1897864.

Mariani, R. D., R. W. Benedict, R. M. Lell, R. B. Turski, and E. K. Fujita. 1996. "Criticality Safety Strategy and Analysis Summary for the Fuel Cycle Facility Electrorefiner at Argonne National Laboratory West." *Nuclear Technology* 114 (2): 224–234. https://doi.org/10.13182/NT96-A35251.

National Research Council. 2000. *Electrometallurgical Techniques for DOE Spent Fuel Treatment: Final Report.* Washington, DC: The National Academies Press. https://doi.org/10.17226/9883.

Neider, T. 2021. *Natrium.* https://www.nationalacademies.org/documents/embed/link/LF2255DA3DD1C41C0A42D3BEF0989ACAECE3053A6A9B/file/D9C4BF4DB67D720A05AD8E65EBD1F70B51F99008B83A?noSaveAs=1.

Peplow, D. E. 2011. "Monte Carlo Shielding Analysis Capabilities with MAVRIC." *Nuclear Technology* 174 (2): 289–313. https://doi.org/10.13182/NT174-289.

Peterson, P. F., H. Zhao, and R. Petroski. 2005. *Metal And Concrete Inputs For Several Nuclear Power Plants.* Technical report UCBTH-05-001. Berkeley, CA: University of California, Berkeley.

Shaw, A., F. Bostelmann, D. Hartanto, E. Walker, and W. A. Wieselquist. 2023. *SCALE Modeling of the Sodium-Cooled Fast-Spectrum Advanced Burner Test Reactor.* Technical report ORNL/TM-2022/2758. Oak Ridge, TN: Oak Ridge National Laboratory. https://doi.org/10.2172/1991734.

Skutnik, S. E., and W. A. Wieselquist. 2021. *Assessment of ORIGEN Reactor Library Development for Pebble-Bed Reactors Based on the PBMR-400 Benchmark.* Technical report ORNL/TM-2020/1886. Oak Ridge, TN: Oak Ridge National Laboratory. https://doi.org/10.2172/1807271.

US NRC. 2020a. *NRC Non-Light Water Reactor (Non-LWR) Vision and Strategy, Volume 3: Computer Code Development Plans for Severe Accident Progression, Source Term, and Consequence Analysis.* Technical report ML20030A178, Rev. 1. Rockville, MD: US Nuclear Regulatory Commission. https://www.nrc.gov/docs/ML2003/ML20030A178.pdf.

US NRC. 2020b. *Standard Review Plan for Transportation Packages for Spent Fuel and Radioactive Material.* Technical report NUREG-2216. Rockville, MD: US Nuclear Regulatory Commission.

US NRC. 2021. *NRC Non-Light Water Reactor (Non-LWR) Vision and Strategy, Volume 5: Radionuclide Characterization, Criticality, Shielding, and Transport in the Nuclear Fuel Cycle.* Technical report ML21088A047, Rev. 1. Rockville, MD: US Nuclear Regulatory Commission. https://www.nrc.gov/docs/ML2108/ML21088A047.pdf.

US NRC, ORNL, SNL. 2023. *SCALE & MELCOR non-LWR Fuel Cycle Demonstration Project - High Temperature Gas-Cooled Reactors.* https://www.nrc.gov/docs/ML2305/ML23058A213.pdf. Accessed: November 6, 2023.

Wagner, J. C., D. E. Peplow, and S. W. Mosher. 2014. "FW-CADIS Method for Global and Regional Variance Reduction of Monte Carlo Radiation Transport Calculations." *Nuclear Science and Engineering* 176 (1): 37–57. https://doi.org/10.13182/NSE12-33.

Wagner, K., B. Beeny, T. Haskin, D. Luxat, and R. Schmidt. 2023. *MELCOR Accident Progression and Source Term Demonstration Calculations for a Molten Salt Reactor.* Technical report SAND2023-01803. Albuquerque, NM: Sandia National Laboratories. https://www.nrc.gov/docs/ML2311/ML23117A094.pdf.

Wagner, K., B. Beeny, and D. Luxat. 2022. *MELCOR Accident Progression and Source Term Demonstration Calculations for a HTGR.* Technical report SAND2022-2750. Albuquerque, NM: Sandia National Laboratories. https://www.osti.gov/biblio/1854083.

Wagner, K., B. Beeny, and D. Luxat. 2023. *MELCOR Accident Progression and Source Term Demonstration Calculations for a Sodium Fast Reactor (SFR).* Technical report SAND2023-10830. Albuquerque, NM: Sandia National Laboratories. https://www.nrc.gov/docs/ML2328/ML23285A093.pdf.

Wagner, K., C. Faucett, R. Schmidt, and D. Luxat. 2022. *MELCOR Accident Progression and Source Term Demonstration Calculations for a Heat Pipe Reactor.* Technical report SAND2022-2745. Albuquerque, NM: Sandia National Laboratories. https://www.osti.gov/biblio/1854082.

Wagner, K., T. Haskin, B. Beeny, F. Gelbard, and D. Luxat. 2022. *MELCOR Accident Progression and Source Term Demonstration Calculations for a FHR.* Technical report SAND2022-2751. Albuquerque, NM: Sandia National Laboratories. https://www.osti.gov/biblio/1854081.

Walker, E., S. E. Skutnik, W. A. Wieselquist, A. Shaw, and F. Bostelmann. 2021. *SCALE Modeling of the Fast-Spectrum Heat Pipe Reactor.* Technical report ORNL/TM-2021/2021. Oak Ridge, TN: Oak Ridge National Laboratory. https://doi.org/10.2172/1871124.

Wieselquist, W., and R. A. Lefebvre. 2023. *SCALE 6.3.1 User Manual.* Technical report ORNL/TM-SCALE-6.3.1. Oak Ridge, TN: Oak Ridge National Laboratory. https://doi.org/10.2172/1959594.